PAPER

Check for updates

Rh-doped MoSe$_2$ as a toxic gas scavenger: a first-principles study

Hao Cui, [ID]^{ab} Guozhi Zhang,^{c} Xiaoxing Zhang [ID] *^{ac} and Ju Tang^c

Using first-principles theory, we investigated the most stable configuration for the Rh dopant on a MoSe$_2$ monolayer, and the interaction of the Rh-doped MoSe$_2$ (Rh-MoSe$_2$) monolayer with four toxic gases (CO, NO, NO$_2$ and SO$_2$) to exploit the potential application of the Rh-MoS$_2$ monolayer as a gas sensor or adsorbent. Based on adsorption behavior comparison with other 2D adsorbents and desorption behavior analysis, we assume that the Rh-MoSe$_2$ monolayer is a desirable adsorbent for CO, NO and NO$_2$ storage or removal given the larger adsorption energy (E_{ad}) of −2.00, −2.56 and −1.88 eV, respectively, compared with other materials. In the meanwhile, the Rh-MoSe$_2$ monolayer is a good sensing material for SO$_2$ detection according to its desirable adsorption and desorption behaviors towards the target molecule. Our theoretical calculation would provide a first insight into the TM-doping effect on the structural and electronic properties of the MoSe$_2$ monolayer, and shed light on the application of Rh-MoSe$_2$ for the sensing or disposal of common toxic gases.

1. Introduction

Sensing toxic gases, especially detection of the ones at sub-ppm levels, is quite imperative with respect to environmental standards and agricultural pollution monitoring. In this regard, researchers have always contributed to finding novel sensing materials for potential application as chemical sensors with a rapid response, high sensitivity and low cost. In the past few decades, semiconducting metal oxide nanowire,[1–3] carbon nanotube,[4–6] and graphene[7–9] based sensors have successively caught the attention of researchers, arousing considerable interest from the research community. Nevertheless, they are never satisfied by these achievements, persisting to pursue some new materials that possess more fascinating sensing behavior than the previous ones.

After the successful application of graphene as a gas sensor, scholars have turned their attention to two-dimensional (2D) materials that have large surface–volume ratios and tunable electronic properties due to their unique structural configuration. Materials such as hexagonal boron nitride,[10] antimonene,[11] phosphorene[12] and silicene[13] have become the focus of the sensing field, in order to find candidate materials having the advantages of graphene such as high carrier mobility and strong chemical activity for gas interaction,[14,15] as well as semiconducting properties. In the meanwhile, group III–V nitrides,

particularly AlN and InN,[16,17] have been regarded as promising structures for gas sensing,[18,19] and the experimental breakthrough in the synthesis of InN[20] makes it possible to be used as a substitute for graphene with inherent bandgap characteristics.[21]

Very recently, 2D transition metal dichalcogenides (TMDs), especially MoS$_2$ monolayers,[22–24] have attracted much attention as alternative materials to conventional metal oxides for chemical sensing devices. Moreover, surface doping with transition metal (TM) atoms has been demonstrated to provide a monolayer with enhanced adsorption and sensing performance for gas molecules[25–28] due to the improved chemical activity and electron mobility induced by the TM dopant,[29] opening up a novel insight into the sensor family. Other than that, MoSe$_2$, as a new emerging semiconducting material, has been investigated as well for its application as a sensor. While Late *et al.* first reported the high sensing performance of the MoSe$_2$ monolayer for ppm-level NH$_3$ gas,[30] Baek *et al.* developed a MoSe$_2$ multilayer based field-effect transistor for NO$_2$ detection.[31] However, the potential applications of MoSe$_2$ based materials need to be further explored and broadened after their successful synthesis by chemical vapor deposition.[32] This inspires us to implement a first-principles calculation to study the adsorption performance of TM-MoSe$_2$ monolayers towards four industrial exhaust gases including CO, NO, NO$_2$ and SO$_2$ to put forward a novel material for toxic gas sensing. Among numerous TM atoms, rhodium (Rh) is the one with strong electron mobility and catalytic performance for gas interaction, previously demonstrated by carbon nanotube,[33] graphene,[34] and MoS$_2$ monolayer systems[35] where Rh was proposed as a dopant to functionalize the proposed surfaces. We assumed that it

^{a}*State Key Laboratory of Power Transmission Equipment & System Security and New Technology, Chongqing University, Chongqing 400044, China. E-mail: xiaoxing. zhang@outlook.com*

^{b}*School of Electrical and Computer Engineering, Georgia Institute of Technology, Atlanta 30332, GA, USA*

^{c}*School of Electrical Engineering, Wuhan University, Wuhan 430072, China*

would be interesting and necessary to investigate the adsorption and sensing behaviors of the Rh-doped $MoSe_2$ (Rh-$MoSe_2$) monolayer towards toxic gases to exploit the novel material for toxic gas detection or removal. The results indicate that the Rh-$MoSe_2$ monolayer possesses quite strong adsorption behavior towards CO, NO and NO_2 molecules that gives rise to chemisorption in these systems, while physisorption could be determined for the Rh-$MoSe_2$/SO_2 system. Through adsorption behavior comparison with other 2D adsorbents and desorption behavior analysis, we assume that Rh-$MoSe_2$ is a desirable adsorbent for CO, NO and NO_2 storage or removal while being a good sensing material for SO_2 detection. To the best of our knowledge, this would be the first report investigating the potential application of Rh-$MoSe_2$ for the removal of four toxic species in a theoretical manner.

2. Computational details

In this work, spin-polarized calculations were implemented in the $Dmol^3$ package[36] of Materials Studio. The Perdew–Burke–Ernzerhof (PBE) functional with a generalized gradient approximation (GGA) was employed to deal with the electron exchange and correlation,[37] and to obtain the optimized structures. The Grimme method was employed[38] for better understanding the van der Waals interaction. We selected double numerical plus polarization (DNP) as the atomic orbital basis set,[26] while the DFT semi-core pseudopotential (DSSP) method was employed to dissolve the relativistic effect of the TM atom.[39] The k-point sample of the Monkhorst–Pack grid was sampled to $5 \times 5 \times 1$ of the Brillouin zone for geometry optimization and to $7 \times 7 \times 1$ for electronic structure calculations.[40] The energy tolerance accuracy, maximum force, and displacement were selected as 10^{-5} Ha, 2×10^{-3} Ha $Å^{-1}$, and 5×10^{-3} Å,[41] respectively. For static electronic structure calculations, a self-consistent loop energy of 10^{-6} Ha, global orbital cut-off radius of 5.0 Å and smearing of 0.005 Ha were employed to ensure the accurate results of total energy.[42] For basis set superposition errors (BSSE), little impact could be caused in the $Dmol^3$ package,[43] and thus we would not analyze it in the following part.

A $4 \times 4 \times 1$ $MoSe_2$ monolayer supercell including 16 Mo and 32 Se atoms with a vacuum region of 15 Å was established and relaxed to its most stable configuration. A previous report has proved that a 4×4 supercell would be large enough to conduct the gas adsorption process while a 15 Å slab would be appropriate to prevent the interaction between adjacent units.[44] The lattice constant calculated here was 3.30 Å, which is in agreement with other theoretical studies (3.31 Å (ref. 45)).

The adsorption energy (E_{ad}) of each gas adsorption process was calculated by the following equation:[23]

$$E_{ad} = E_{Rh\text{-}MoSe_2/gas} - E_{Rh\text{-}MoSe_2} - E_{gas} \qquad (1)$$

where the $E_{Rh\text{-}MoSe_2/gas}$, $E_{Rh\text{-}MoSe_2}$ and E_{gas} represent energies of the adsorbed system, isolated Rh-$MoSe_2$ and gas molecule, respectively. To analyze the charge transfer (Q_T) between the target molecule and adsorbent surface, the Mulliken population

analysis was considered, characterized by the carried electron value by gas molecules after adsorption. Only the most favorable configuration for gas adsorption would be plotted and analyzed in the following parts.

3. Results and discussion

3.1 Geometric and electronic structure of Rh-$MoSe_2$

We determined Rh atom adsorption onto a bare $MoSe_2$ monolayer Rh-$MoSe_2$, where four possible sites were considered, traced as T_H (above the center of the hexagonal ring of $MoSe_2$), T_{Mo} (at the top of the Mo atom), T_{Se} (at the top of the Se atom) and B_{S-S} (the bridge site between two Se atoms), respectively. The binding energy (E_b) for Rh adsorption onto the most favorable doping site is determined through the formula:

$$E_d = E_{Rh\text{-}MoSe_2} - E_{Rh} - E_{MoSe2} \qquad (2)$$

where $E_{Rh\text{-}MoSe_2}$, E_{Rh}, and E_{MoSe_2} represent the energies of the Rh-$MoSe_2$, Rh atom and pure $MoSe_2$, respectively.

After optimization, the most stable configuration of Rh-$MoSe_2$ in line with relevant deformation charge density (DCD) is shown in Fig. 1. One can see that the Rh atom tends to be adsorbed onto the $MoSe_2$ monolayer through the T_{Mo} site, with three Rh–Se bond lengths of 2.383, 2.383 and 2.354 Å, respectively. The geometry of $MoSe_2$ undergoes a little deformation after Rh doping due to the binding force of Rh–Se bonds.[46] The Q_T between the Rh dopant and the $MoSe_2$ monolayer is found to be −0.239 e, indicating that the Rh dopant acts as an electron acceptor while the $MoSe_2$ monolayer acts as a donor. This is in line with the strong electron withdrawing properties of the Rh atom,[33] thereby leading to high electron localization around the Rh atom. In addition, we can find that the Mo atoms are mainly the electron accepting centers while the Se atoms are the electron donating centers for the optimized Rh-$MoSe_2$ system.
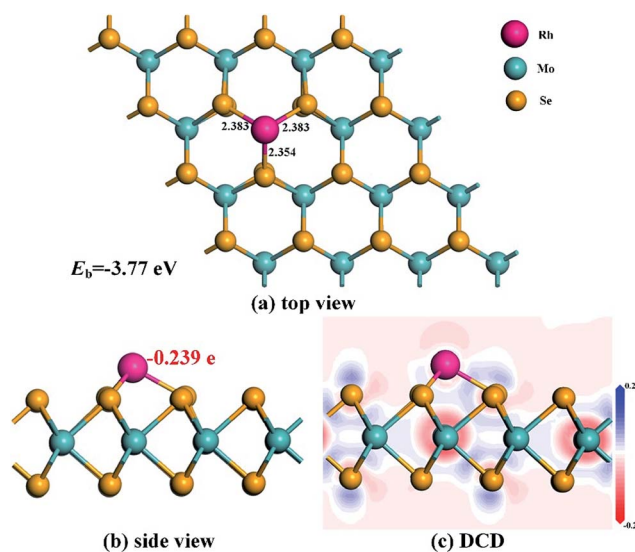

Fig. 1 Geometric structures (a) and (b) and DCD (c) of the Rh-$MoSe_2$ monolayer. The black values are the atom-to-atom distance while the red value is the electron amount carried by Rh dopant.

To further elucidate the electronic behavior of the Rh doping effect on the $MoSe_2$ monolayer compared with its pure counterpart, density of states (DOS) analysis is performed, as depicted in Fig. 2. It can be seen in the total DOS distribution of Fig. 2(a) that there is a big band gap near the Fermi level in the DOS curve of intrinsic $MoSe_2$, confirming its semiconducting properties well. With the doping of the Rh atom, the gap gets narrowed obviously due to the upward shifted Fermi level which was originally identified as the valence band maximum in the $Dmol^3$ package, caused by the Rh contribution. It is interesting to note that the DOS spin up and down of the Rh-$MoSe_2$ monolayer are shown to be asymmetric in comparison with those in the pure $MoSe_2$ system that shows good symmetry, which could be ascribed to the total magnetic moment of 1.0 μ_B in this system induced by the Rh dopant. Moreover, due to the electron-donating behavior of the $MoSe_2$ monolayer that results in an improved effective coulombic potential,[47] the DOS curve of the Rh-$MoSe_2$ system is found to left shift towards a lower region consequently compared with that of its intrinsic counterpart. In Fig. 1(b), the DOS of the Rh 4d orbital is largely overlapped with that of the Se 4p orbital, demonstrating strong hybridization of the Rh atom onto the $MoSe_2$ monolayer. Apart from that, it reveals that the highest occupied molecular orbitals (HOMOs) are mainly located at the Se atom while the lowest unoccupied molecular orbitals are at the Rh atom, which confirms the results of DCD that charge is accumulated around the Rh dopant.[48]

3.2 CO adsorption

Fig. 3 shows the most stable configuration and related DCD for CO adsorption on the Rh-$MoSe_2$ monolayer. One can see that the C atom is trapped by the Rh dopant with a Rh–C bond length of 1.892 Å after the CO molecule is adsorbed on the
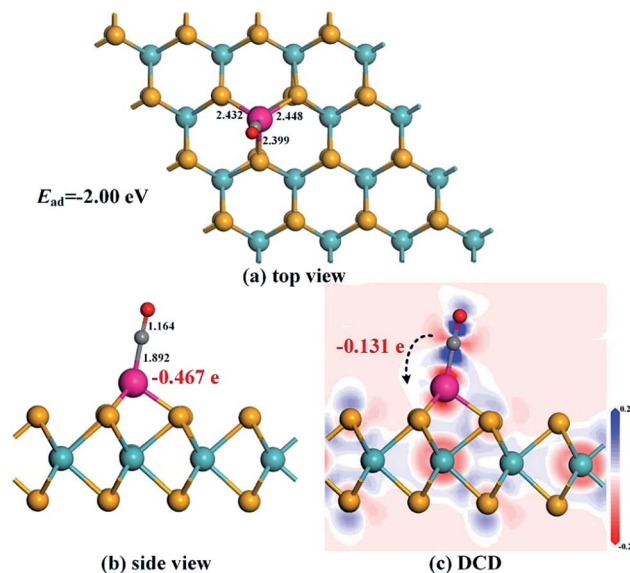

Fig. 3 Adsorption configuration (a) and (b) and DCD (c) of the Rh-$MoSe_2$/CO system.

surface. It would be worth noting that such a value of atom-to-atom distance is even shorter than the sum of the corresponding covalent radii (2.00 Å for Rh–C[49]) indicating some chemisorption in this system.[50] In fact, the large enough E_{ad} of −2.00 eV here could not only confirm the strong adsorption performance of Rh-$MoSe_2$ towards the CO molecule, but also indicate its chemical nature with strong spontaneity for this interaction. In the meanwhile, three Rh–Se bonds, after CO adsorption, are elongated to 2.432, 2.448 and 2.399 Å, respectively, and the C–O bond of the CO molecule is prolonged to 1.164 Å from 1.142 Å in an isolated molecule. These findings suggest the activation behavior for the CO molecule when interacted with the
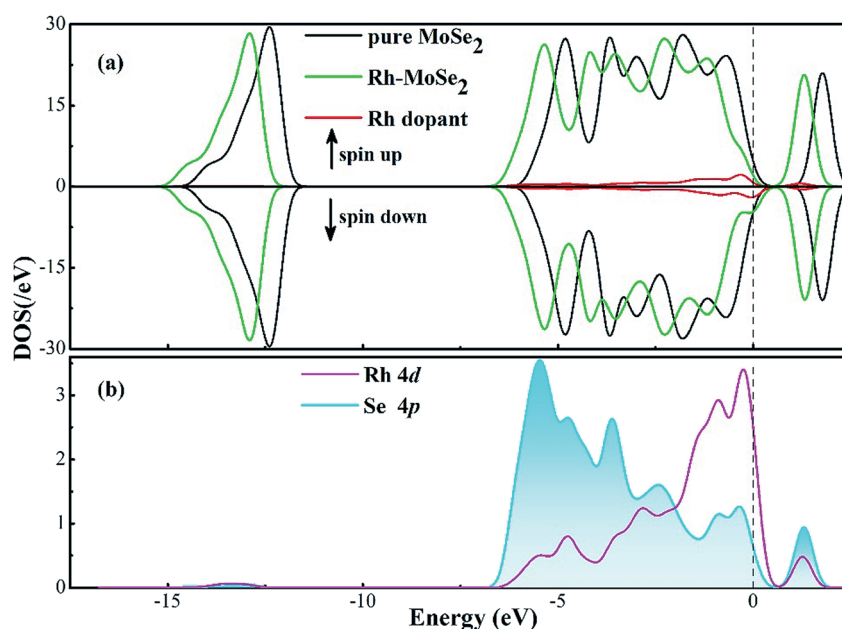

Fig. 2 DOS distribution of Rh-$MoSe_2$. The dashed line is the Fermi level.

monolayer. The DCD shows that the Rh-MoSe$_2$ monolayer acting as an electron acceptor withdraws 0.131 e from the adsorbed CO molecule. This, combined with the Mulliken population analysis for the Rh dopant that carries 0.467 e after adsorption, indicates that the Rh dopant is an electron localization center accepting charge from both gas molecules and the MoSe$_2$ surface.

Fig. 4 shows the total and partial DOS distributions for the CO adsorption system. Based on the comparison between the total DOS for the pure Rh-MoSe$_2$ system and the one for the adsorbed system, we can find that they are basically overlapped except for the area near the Fermi levels where the Rh dopant contributes a lot due to its strong electron activity, and the areas at 6.5 and 8.5 eV where the adsorbed CO molecule makes a great contribution for the DOS of the whole system. Besides, the deformations for the DOS between the isolated CO molecule and the adsorbed one confirm that the CO molecule is activated during gas adsorption. Moreover, the large overlaps between DOS of Rh 4d and C 2p orbitals manifest strong hybridization between Rh and C atoms, which would explain the strong binding force of the Rh–C bond that leads to the short atom-to-atom distance.

3.3 NO adsorption

The most stable adsorption configuration and related DCD for the Rh-MoSe$_2$/NO system are exhibited in Fig. 5. One can observe that the structure for NO adsorption onto the Rh-MoSe$_2$ monolayer, with N atoms captured, is somewhat similar to that of the CO system. However, the largely elongated Rh–Se bonds with lengths of 2.445, 2.453 and 2.449 Å in the NO system
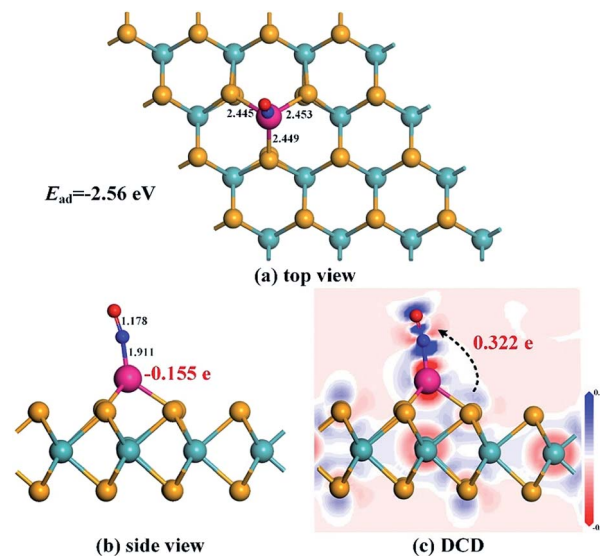

Fig. 5 Adsorption configuration (a) and (b) and DCD (c) of the Rh-MoSe$_2$/NO system.

suggest a stronger binding force of Rh on the NO molecule than the CO molecule. Similarly, the elongated N–O bond of 1.178 Å in the adsorbed NO molecule in comparison with its isolated counterpart (1.164 Å) indicates the activation behavior of the NO molecule for interaction with the Rh-MoSe$_2$ monolayer.[35] The shorter length of the Rh–N bond (1.911 Å) compared with the sum of relevant covalent radii (1.96 Å for Rh–N[49]) shows the nature of chemisorption. In fact, all these results could be well supported by the large E_{ad} of −2.56 eV and Q_T of −0.322 e calculated in this system as they are large enough to confirm the strong interaction between gas molecules and the adsorbent surface.[51]

From the DOS distribution for the NO system as portrayed in Fig. 6, the electronic behavior for NO adsorption on the Rh-MoSe$_2$ monolayer could be elucidated clearly. In the total DOS distribution, we can see that the DOS of the NO system transforms slightly above the Fermi level compared with that of the pure Rh-MoSe$_2$ system. In detail, two novel peaks appear at around −7.5 and −8.5 eV while one peak at the Fermi level disappears after gas adsorption, which could be attributed to the DOS deformation of the adsorbed NO molecule. It could be seen that the DOS peak of the isolated NO molecule at the Fermi level splits into two small peaks after NO adsorption that weakens the contribution to the total DOS of the whole system, while the slightly weakened peak at −8.5 eV and the enhanced peak at −7.5 eV accord with the novel peaks in DOS for the adsorbed system. Based on the partial DOS analysis, we could see that every peak of the N 2p orbital is overlapped with that of the Rh 4d orbital, implying that the N atom is strongly hybridized with the Rh dopant, thus giving rise to a strong binding force for the Rh–N bond.
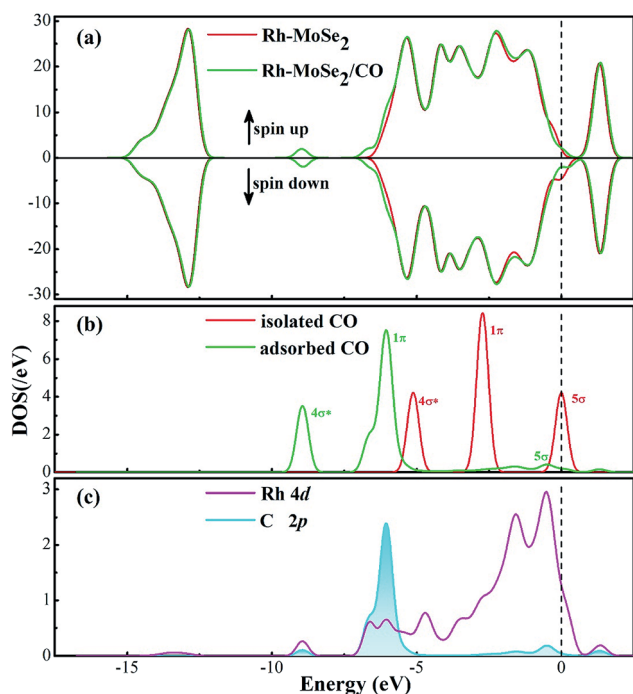

Fig. 4 DOS distribution of the Rh-MoSe$_2$/CO system. The dashed line is the Fermi level. In the gas DOS, the red value shows the orbitals of isolated molecules while the green one shows the orbitals of adsorbed molecules.

3.4 NO$_2$ adsorption

In terms of NO$_2$ adsorption onto the Rh-MoSe$_2$ monolayer, one can see from Fig. 7 that the NO$_2$ molecule prefers to adsorb two

Fig. 6 DOS distribution of the Rh-MoSe$_2$/NO system. The dashed line is the Fermi level. In the gas DOS, the red value shows the orbitals of isolated molecules while the green one shows the orbitals of adsorbed molecules.
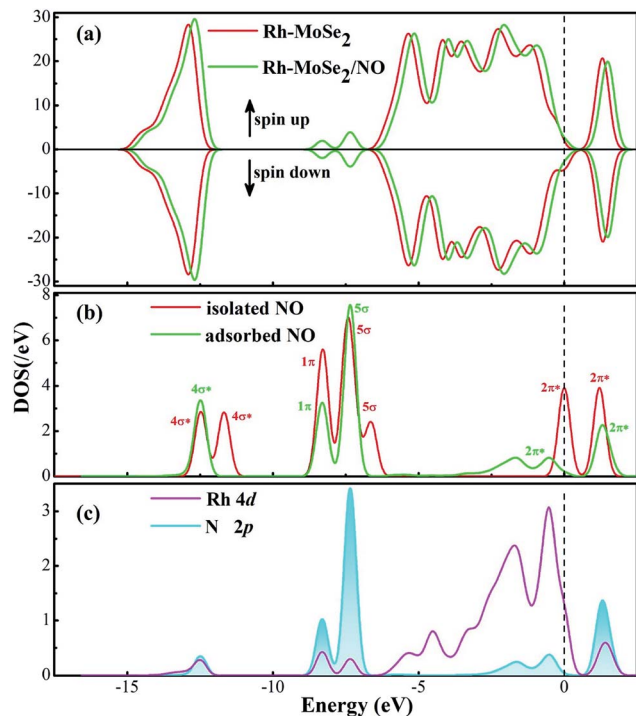
O atoms trapped with a shorter Rh–O distance of 2.113 Å. Three Rh–Se bonds of Rh-MoSe$_2$ in line with the N–O bond of the NO$_2$ molecule undergo some elongation after adsorption, due to the binding force of Rh on the NO$_2$ molecule. The Mulliken population analysis indicates that 0.361 e transfers from the Rh-MoSe$_2$ monolayer to the NO$_2$ molecule with an electron loss of 0.086 for the Rh dopant. That is to say, unlike in the CO system, the Rh dopant acts as an electron donor releasing the
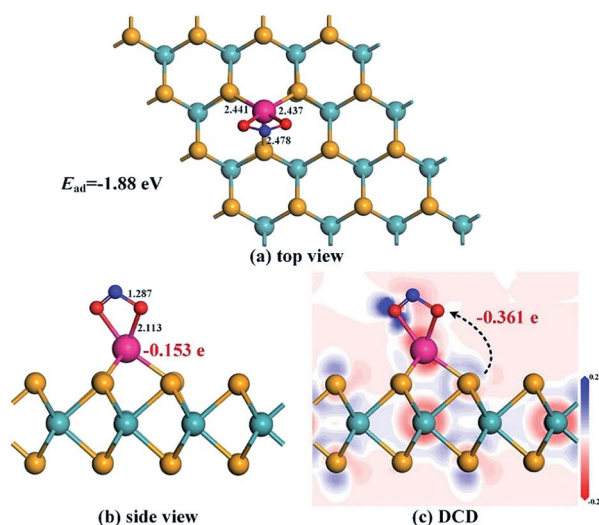
electron to the gas molecule, which could be found in NO and SO$_2$ systems as well. This finding manifests the strong electron mobility and chemical activity of TM when interacting with gas molecules.[52] Moreover, the large Q_T associated with the relatively large E_{ad} suggests the kind of chemisorption for the Rh-MoSe$_2$/NO$_2$ system.

Fig. 8 shows the DOS distributions for the NO$_2$ adsorption system. One can find from the total DOS configurations that the DOS curve transforms dramatically around the Fermi level after adsorption of the NO$_2$ molecule. This may be attributed to the considerable electron-transfer between gas molecules and the adsorbent surface that results in electron redistribution for the whole system, thus leading to the deformation of electronic states at the Fermi level.[53] Furthermore, the novel emerged peaks at −7.5, −8.5 and −11.5 eV are contributed by the adsorbed NO$_2$ molecule which is activated during adsorption. Similarly, the hybridization between Rh and O atoms is identified through the phenomenon of overlaps between Rh 4d and O 2p orbitals.

3.5 SO$_2$ adsorption

From Fig. 9 where the most stable configuration for SO$_2$ adsorption on the Rh-MoSe$_2$ monolayer is displayed, we can see that, similar to the NO$_2$ adsorption configuration, the SO$_2$ molecule is adsorbed on the Rh-MoSe$_2$ monolayer with two O atoms oriented. However, the SO$_2$ molecule here stands a little far from the Rh dopant, with the nearest atom-to-atom distance measured to be 2.275 Å, which indicates a weak interaction in
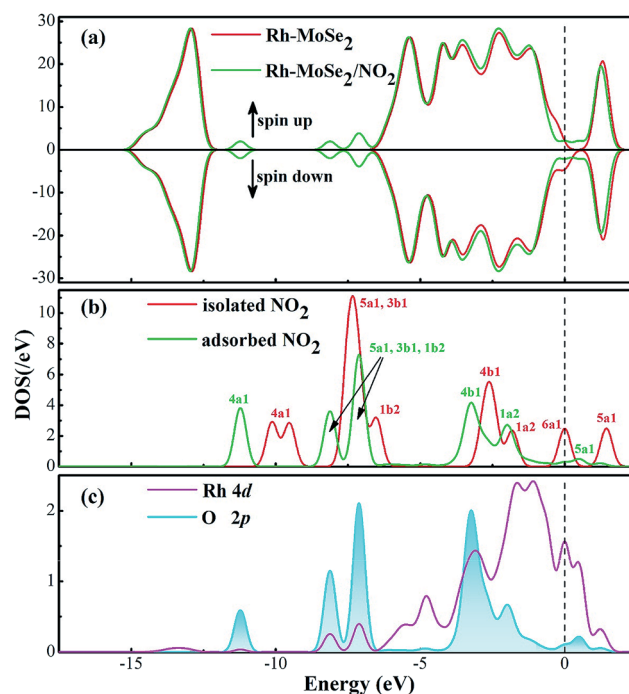

Fig. 7 Adsorption configuration (a) and (b) and DCD (c) of the Rh-MoSe$_2$/NO$_2$ system.

Fig. 8 DOS distribution of the Rh-MoSe$_2$/NO$_2$ system. The dashed line is the Fermi level. In the gas DOS, the red value shows the orbitals of isolated molecules while the green one shows the orbitals of adsorbed molecules.
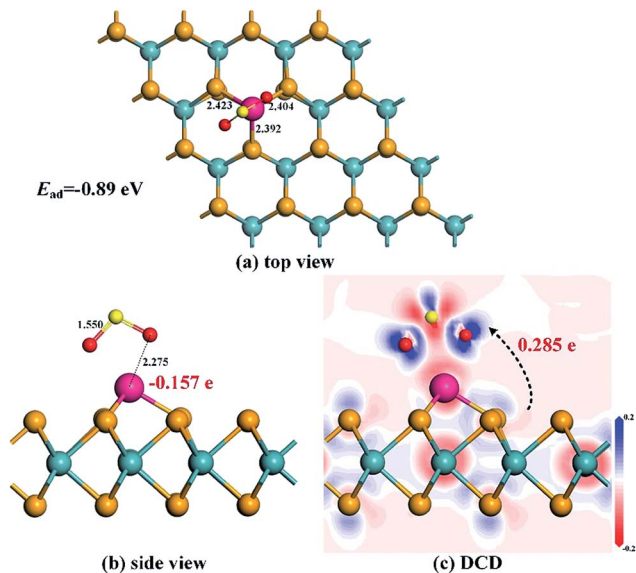
Fig. 9 Adsorption configuration (a) and (b) and DCD (c) of the Rh–MoSe$_2$/SO$_2$ system.

the Rh-MoSe$_2$/SO$_2$ system. The tiny prolongation for Rh–Se bonds inner Rh-MoSe$_2$ to 2.423, 2.404 and 2.392 Å, along with S–O bond inner SO$_2$ to 1.550 Å by 0.019 Å can confirm the weak binding force between the Rh dopant and the SO$_2$ molecule as well. The E_{ad} obtained here is −0.89 eV and the Mulliken population analysis shows a Q_T of 0.285 e from the Rh-MoSe$_2$ monolayer to the SO$_2$ molecule. All these findings suggest physisorption for SO$_2$ adsorption on the Rh-MoSe$_2$ monolayer.[51]

DOS distributions shown in Fig. 10 could give a clear explanation for the electronic behavior in this system. The novel peaks around −11.5 and −7 and the Fermi level in total DOS of the adsorbed system are from the contribution of the adsorbed SO$_2$ molecule that is somewhat activated after adsorption. At the same time, the overlaps between DOS of Rh 4d and O 2p orbitals, although not as large as the NO$_2$ system, prove the orbital interaction, to some extent, between the Rh dopant and the SO$_2$ molecule.

3.6 Application of Rh-MoSe$_2$ to toxic gas scavenging

We first investigated the potential application of Rh-MoSe$_2$ as a resistance-type sensor for these gases. According to our previous analysis, it could be found that the Rh-MoSe$_2$ monolayer has quite strong adsorption performance for three species namely CO, NO and NO$_2$ molecules, giving rise to chemisorption in these systems, while having relatively weaker performance towards SO$_2$ adsorption that gives rise to physisorption instead. In other words, it would be difficult for these three gas molecules to desorb from the Rh-MoSe$_2$ monolayer once they are adsorbed onto the surface, except for the SO$_2$ molecule which may be desorbed through annealing at high temperature or irradiation with ultraviolet light.[50,54]

To confirm this assumption, the recovery time (τ) analysis based on transition state theory and van't-Hoff–Arrhenius expression[55] was implemented, and expressed as:
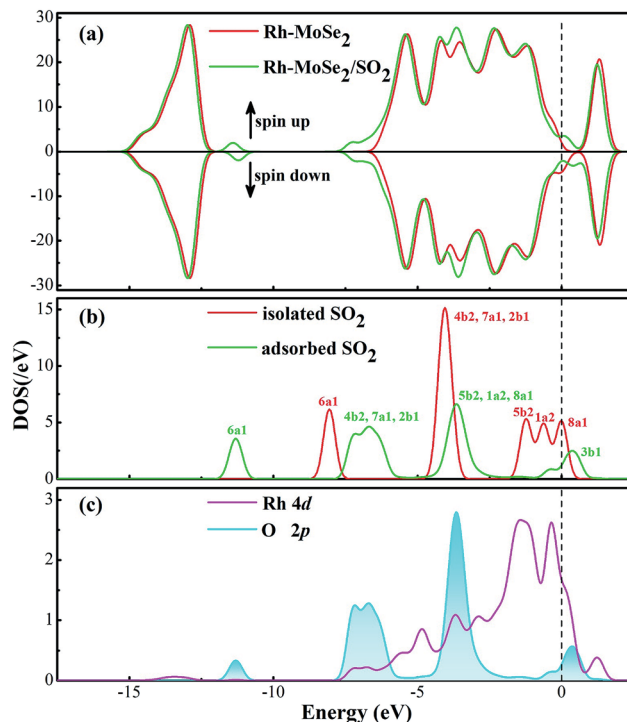

Fig. 10 DOS distribution of the Rh-MoSe$_2$/SO$_2$ system. The dashed line is the Fermi level.

$$\tau = A^{-1} e^{(-E_a/K_B T)} \tag{3}$$

where A is the attempt frequency determined as 10^{12} s^{-1} according to a previous report,[56] T is the temperature and K_B is the Boltzmann constant (8.318×10^{-3} kJ (mol K)$^{-1}$). Given the inverse processes between adsorption and desorption, we assume the value of E_{ad} as the potential barrier (E_a) for desorption. It would be obvious that a larger E_{ad} would lead to a harder process for gas desorption, and the increase of temperature can accelerate that process effectively. According to the obtained E_{ad} in our calculations as shown in Table 1, we plotted the recovery time for the desorption of various gases at various temperatures as portrayed in Fig. 11. One can conclude that CO, NO and NO$_2$ desorption from the Rh-MoSe$_2$ monolayer would be extremely unrealistic at room temperature, and even at 798 K, it would take more than 4 hours for NO desorption from the surface. Although remarkably enhanced behavior for CO and NO$_2$ desorption could be achieved at 798 K, the considerable heat loss and the safety of the devices would be another issue. Therefore, it would be inappropriate to use the Rh-MoSe$_2$ monolayer as the sensing material for CO, NO or NO$_2$ detection, because the one-off operation for gas sensors would be a waste of money and reduce work-efficiency. On the other hand, we assume that Rh-MoSe$_2$ is suitable for SO$_2$ sensing given its good adsorption performance for detection and desorption performance with appropriate recovery time at ambient temperature for recycle use. Moreover, the sensing mechanism of the Rh-MoSe$_2$ monolayer towards SO$_2$ would be dependent on the increased conductivity due to the narrowed energy gap from 1.033 eV for the isolated Rh-MoSe$_2$ monolayer to 0.227 eV for the SO$_2$ system[57] as seen in Table 1.

Table 1 Adsorption parameters for various Rh–MoSe$_2$/gas systems

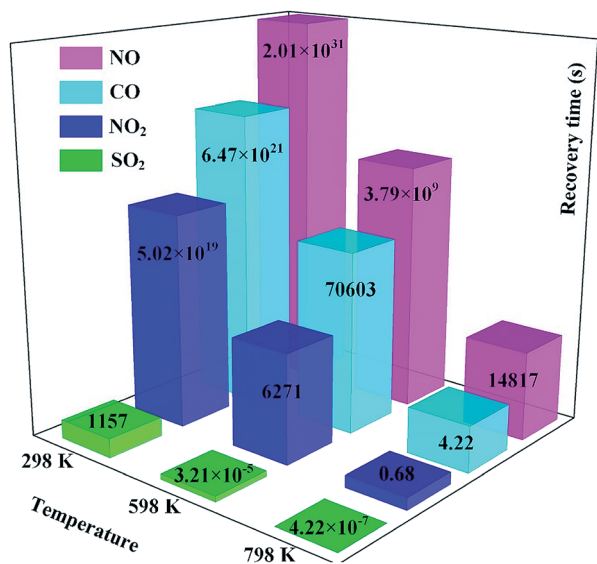| Gas systems	E_{ad} (eV)	D (Å)	Q_T (e)	E_g (eV)
CO	−2.00	1.892	−0.131	0.202
NO	−2.56	1.911	0.322	1.210
NO$_2$	−1.88	2.113	−0.361	0.520
SO$_2$	−0.89	2.275	0.285	0.227

Fig. 11 Recovery time for four species at various temperatures.

Second, the large E_{ad} in CO, NO and NO$_2$ systems allows the excellent performance of Rh–MoSe$_2$ as a gas adsorbent for their storage or removal from specific environments. For this purpose, we summarize in Fig. 12 the calculated E_{ad} values of recently reported 2D adsorbents for four gases, in order to find out whether Rh–MoSe$_2$ could be an alternative for scavenging toxic gases. From the figure, we can find that the Rh–MoSe$_2$ monolayer possesses better adsorption performance for CO, NO and NO$_2$ molecules compared with the pure MoS$_2$ monolayer,[23] the pure MoSe$_2$ monolayer,[58] pure InN,[19] pure C$_3$N,[57] pure penta-graphene,[59] and some other TM-doped MoS$_2$ monolayers.[22,40,60,61] That is to say, the Rh–MoSe$_2$ monolayer has strong potential to be an adsorbent candidate for CO, NO or NO$_2$ storage and removal. Conversely, it is not a desirable SO$_2$ adsorbent due to its weaker performance than pure InN,[19] penta-graphene,[59] the Au–MoS$_2$ monolayer,[40] the Pt–MoS$_2$ monolayer[40] and the Ni–MoS$_2$ monolayer,[60] although it has better performance than the pure MoS$_2$ monolayer,[23] the pure MoSe$_2$ monolayer[58] and pure C$_3$N,[57] except for the Cu–MoS$_2$ monolayer which is not studied for SO$_2$ adsorption in ref. 22 and 61. In addition, we would introduce the application of borophene as a potential SO$_2$ adsorbent given its strong ability and capacity whereby up to seven SO$_2$ molecules could be chemisorbed on its one side, with a weight percentage of 82.88%, for SO$_2$ adsorption.[62]
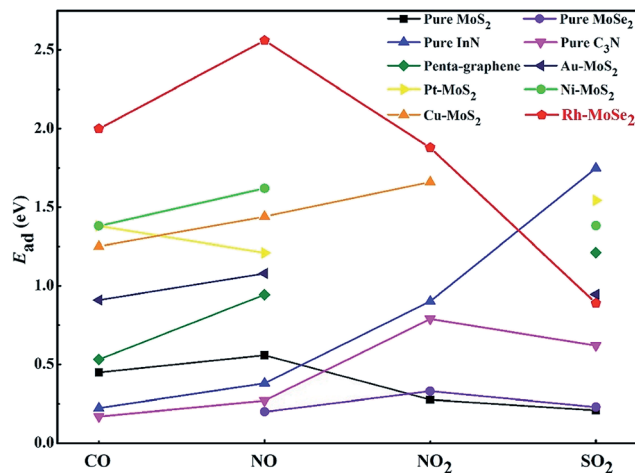
Fig. 12 E_{ad} comparison of Rh–MoSe$_2$ for four species with recent reports.

4. Conclusions

In this work, we implemented a first-principles theory to study the adsorption performance of the Rh–MoSe$_2$ monolayer towards four toxic gases, including CO, NO, NO$_2$ and SO$_2$. Desorption behavior analysis and adsorption behavior comparison with other 2D materials towards these four species were conducted in order to exploit the potential application of our proposed monolayer. The results indicated that the Rh–MoSe$_2$ monolayer possesses quite strong adsorption behavior towards CO, NO and NO$_2$ molecules that gives rise to chemisorption in these systems, while physisorption could be determined for the Rh–MoSe$_2$/SO$_2$ system. In that regard, based on the adsorption behavior comparison with other adsorbents and desorption behavior analysis, we assume that Rh–MoSe$_2$ is a desirable adsorbent for CO, NO and NO$_2$ storage or removal while it is a good sensing material for SO$_2$ detection. Our theoretical calculation would provide a first insight into the TM-doping effect on the structural and electronic properties of the MoSe$_2$ monolayer, and shed light on the application of Rh–MoSe$_2$ for the sensing or disposal of common toxic gases.

Author contributions

Xiaoxing Zhang conceived and designed the research, Hao Cui performed the research and wrote this manuscript while Guozhi Zhang and Ju Tang helped analyze the data.

Conflicts of interest

There are no conflicts to declare.

Acknowledgements

References

1 X. Li, Z. Gu, J. H. Cho, H. Sun and P. Kurup, Tin–copper mixed metal oxide nanowires: synthesis and sensor response to chemical vapors, *Sens. Actuators, B*, 2011, **158**(1), 199–207.

2 H. S. Woo, W. N. Chan and J. H. Lee, Design of Highly Selective Gas Sensors *via* Physicochemical Modification of Oxide Nanowires: Overview, *Sensors*, 2016, **16**(9), 1531.

3 C. Sun, G. Maduraiveeran and P. Dutta, Nitric oxide sensors using combination of p- and n-type semiconducting oxides and its application for detecting NO in human breath, *Sens. Actuators, B*, 2013, **186**(18), 117–125.

4 M. Mittal and A. Kumar, Carbon nanotube (CNT) gas sensors for emissions from fossil fuel burning, *Sens. Actuators, B*, 2014, **203**, 349–362.

5 T. Zhang, S. Mubeen, N. V. Myung and M. A. Deshusses, Recent progress in carbon nanotube-based gas sensors, *Nanotechnology*, 2008, **19**(33), 332001.

6 C. Gao, Z. Guo, J. H. Liu and X. J. Huang, The new age of carbon nanotubes: an updated review of functionalized carbon nanotubes in electrochemical sensors, *Nanoscale*, 2012, **4**(6), 1948–1963.

7 Y. Tang, W. Chen, C. Li, L. Pan, X. Dai and D. Ma, Adsorption behavior of Co anchored on graphene sheets toward NO, SO_2, NH_3, CO and HCN molecules, *Appl. Surf. Sci.*, 2015, **342**, 191–199.

8 M. Zhou, Y. H. Lu, Y. Q. Cai, C. Zhang and Y. P. Feng, Adsorption of gas molecules on transition metal embedded graphene: a search for high-performance graphene-based catalysts and gas sensors, *Nanotechnology*, 2011, **22**(38), 385502.

9 Y. Liu, X. Dong and P. Chen, ChemInform Abstract: Biological and Chemical Sensors Based on Graphene Materials, *Chem. Soc. Rev.*, 2012, **41**(6), 2283–2307.

10 T. A. Abtew, W. Gao, X. Gao, Y. Y. Sun, S. B. Zhang and P. Zhang, Theory of Oxygen-Boron Vacancy Defect in Cubic Boron Nitride: A Diamond NV^- Isoelectronic Center, *Phys. Rev. Lett.*, 2014, **113**(13), 136401.

11 S. Zhang, Z. Yan, Y. Li, Z. Chen and H. Zeng, Atomically thin arsenene and antimonene: semimetal–semiconductor and indirect–direct band-gap transitions, *Angew. Chem.*, 2015, **54**(10), 3112.

12 S. Zhang, S. Guo, Z. Chen, Y. Wang, H. Gao, J. Gómez-Herrero, P. Ares, F. Zamora, Z. Zhu and H. Zeng, Recent progress in 2D group-VA semiconductors: from theory to experiment, *Chem. Soc. Rev.*, 2018, **47**(3), 982–1021.

13 H. F. Dai, P. Xiao and Q. Lou, Application of SnO_2/MWCNTs nanocomposite for SF_6 decomposition gas sensor, *Phys. Status Solidi*, 2011, **208**(7), 1714–1717.

14 S. V. Morozov, K. S. Novoselov, M. I. Katsnelson, F. Schedin, D. C. Elias, J. A. Jaszczak and A. K. Geim, Giant intrinsic carrier mobilities in graphene and its bilayer, *Phys. Rev. Lett.*, 2008, **100**(1), 016602.

15 Y. H. Zhang, Y. B. Chen, K. G. Zhou, C. H. Liu, J. Zeng, H. L. Zhang and Y. Peng, Improving gas sensing properties of graphene by introducing dopants and defects: a first-principles study, *Nanotechnology*, 2009, **20**(18), 185504.

16 C. Bungaro, K. Rapcewicz and J. Bernholc, *Ab initio* phonon dispersions of wurtzite AlN, GaN, and InN, *Phys. Rev. B: Condens. Matter Mater. Phys.*, 2000, **61**(10), 6720–6725.

17 C. Stampfl, C. G. de Walle Van, D. Vogel, P. Krüger and J. Pollmann, Native defects and impurities in InN: first-principles studies using the local-density approximation and self-interaction and relaxation-corrected pseudopotentials, *Phys. Rev. B: Condens. Matter Mater. Phys.*, 2000, **61**(12), 52–56.

18 S. F. Rastegar, A. A. Peyghan, H. R. Ghenaatian and N. L. Hadipour, NO_2 detection by nanosized AlN sheet in the presence of NH_3: DFT studies, *Appl. Surf. Sci.*, 2013, **274**(5), 217–220.

19 X. Sun, Q. Yang, R. Meng, C. Tan, Q. Liang, J. Jiang, H. Ye and X. Chen, Adsorption of gas molecules on graphene-like InN monolayer: a first-principle study, *Appl. Surf. Sci.*, 2017, **404**, 291–299.

20 H. Y. Xu, Z. Liu, X. T. Zhang and S. K. Hark, Synthesis and optical properties of InN nanowires and nanotubes, *Appl. Phys. Lett.*, 2007, **90**(11), R1.

21 C. E. P. Villegas and A. R. Rocha, Elucidating the Optical Properties of Novel Heterolayered Materials Based on $MoTe_2$–InN for Photovoltaic Applications, *J. Phys. Chem. C*, 2015, **119**(21), 150513134853008.

22 S. Archana, Anu, M. Shahid Khan, M. Husain, Md. Shahzad Khan and A. Srivastava, Sensing of CO and NO on Cu-doped MoS_2 Monolayer Based Single Electron Transistor: A First Principles Study, *IEEE Sens. J.*, 2018, (99), 1.

23 A. Shokri and N. Salami, Gas sensor based on MoS_2 monolayer, *Sens. Actuators, B*, 2016, **236**, 378–385.

24 D. Ma, Q. Wang, T. Li, C. He, B. Ma, Y. Tang, Z. Lu and Z. Yang, Repairing sulfur vacancies in the MoS_2 monolayer by using CO, NO and NO_2 molecules, *J. Mater. Chem. C*, 2016, **4**(29), 7093–7101.

25 D. Ma, W. Ju, T. Li, X. Zhang, C. He, B. Ma, Z. Lu and Z. Yang, The adsorption of CO and NO on the MoS_2 monolayer doped with Au, Pt, Pd, or Ni: a first-principles study, *Appl. Surf. Sci.*, 2016, **383**, 98–105.

26 D. Zhang, J. Wu, L. Peng and Y. Cao, Room-temperature SO_2 gas-sensing properties based on a metal-doped MoS_2 nanoflower: an experimental and density functional theory investigation, *J. Mater. Chem. A*, 2017, **5**(39), 20666–20677.

27 L. Zhansheng, P. Lv, D. Ma, X. Yang, S. Li and Z. Yang, Detection of gas molecules on single Mn adatom adsorbed graphyne: a DFT-D study, *J. Phys. D: Appl. Phys.*, 2018, **51**(6), 065109.

28 D. Ma, W. Ju, T. Li, G. Yang, C. He, B. Ma, Y. Tang, Z. Lu and Z. Yang, Formaldehyde molecule adsorption on the doped monolayer MoS_2: a first-principles study, *Appl. Surf. Sci.*, 2016, **371**, 180–188.

29 D. Ma, W. Ju, T. Li, X. Zhang, C. He, B. Ma, Y. Tang, Z. Lu and Z. Yang, Modulating electronic, magnetic and chemical properties of MoS_2 monolayer sheets by substitutional doping with transition metals, *Appl. Surf. Sci.*, 2016, **364**, 181–189.

30 D. J. Late, T. Doneux and M. Bougouma, Single-layer MoSe$_2$ based NH$_3$ gas sensor, *Appl. Phys. Lett.*, 2014, **105**(23), 25.

31 J. Baek, D. Yin, N. Liu, I. Omkaram, C. Jung, I. Healin, S. Hong, S. M. Kim, Y. K. Hong, J. Hur, Y. Yoon and S. Kim, A highly sensitive chemical gas detecting transistor based on highly crystalline CVD-grown MoSe$_2$ films, *Nano Res.*, 2017, **10**(8), 2904.

32 S. Y. Choi, Y. Kim, H. S. Chung, A. R. Kim, J. D. Kwon, J. Park, Y. L. Kim, S. H. Kwon, M. G. Hahm and B. Cho, Effect of Nb Doping on Chemical Sensing Performance of Two-Dimensional Layered MoSe$_2$, *ACS Appl. Mater. Interfaces*, 2017, **9**(4), 3817–3823.

33 S. Li and J. Jiang, Adsorption behavior analyses of several small gas molecules onto Rh-doped single-walled carbon nanotubes, *Appl. Phys. A: Mater. Sci. Process.*, 2017, **123**(10), 669.

34 M. Giovanni, H. L. Poh, A. Ambrosi, G. Zhao, Z. Sofer, F. Šaněk, B. Khezri, R. D. Webster and M. Pumera, Noble metal (Pd, Ru, Rh, Pt, Au, Ag) doped graphene hybrids for electrocatalysis, *Nanoscale*, 2012, **4**(16), 5002–5008.

35 Y. Fan, J. Zhang, Y. Qiu, Z. Jia, Y. Zhang and G. Hu, A DFT study of transition metal (Fe, Co, Ni, Cu, Ag, Au, Rh, Pd, Pt and Ir)-embedded monolayer MoS$_2$ for gas adsorption, *Comput. Mater. Sci.*, 2017, **138**, 255–266.

36 B. Delley, From molecules to solids with the DMol^3 approach, *J. Chem. Phys.*, 2000, **113**(18), 7756–7764.

37 H. Cui, X. Zhang, D. Chen, J. Tang. Adsorption mechanism of SF$_6$ decomposed species on pyridine-like PtN$_3$ embedded CNT: a DFT study. Applied Surface Science, 2018, 447.

38 A. Tkatchenko, R. Di Stasio Jr, M. Head-Gordon and M. Scheffler, Dispersion-corrected Møller–Plesset second-order, *J. Chem. Phys.*, 2009, **131**(9), 171.

39 B. Delley, Hardness conserving semilocal, *Phys. Rev. B: Condens. Matter Mater. Phys.*, 2002, **66**(15), 155125.

40 D. Chen, X. Zhang, J. Tang, H. Cui and Y. Li, Noble metal (Pt or Au)-doped monolayer MoS$_2$ as a promising adsorbent and gas-sensing material to SO$_2$, SOF$_2$ and SO$_2$F$_2$: a DFT study, *Appl. Phys. A: Mater. Sci. Process.*, 2018, **124**(2), 194.

41 H. Cui, X. Zhang, J. Zhang and J. Tang, Adsorption behaviour of SF$_6$ decomposed species onto Pd$_4$-decorated single-walled CNT: a DFT study, *Mol. Phys.*, 2018, (53), 1–7.

42 W. Ju, T. Li, X. Su, H. Li, X. Li and D. Ma, Au cluster adsorption on perfect and defective MoS$_2$ monolayers: structural and electronic properties, *Phys. Chem. Chem. Phys.*, 2017, **19**, 20735–20748.

43 S. G. Lee, J. Il Choi, W. Koh and S. S. Jang, Adsorption of β-D-glucose and cellobiose on kaolinite surfaces: density functional theory (DFT) approach, *Appl. Clay Sci.*, 2013, **71**, 73–81.

44 P. Wu, N. Yin, P. Li, W. Cheng and M. Huang, The adsorption and diffusion behavior of noble metal adatoms (Pd, Pt, Cu, Ag and Au) on a MoS$_2$ monolayer: a first-principles study, *Phys. Chem. Chem. Phys.*, 2017, **19**(31), 20713–20722.

45 Y. Ma, Y. Dai, M. Guo, C. Niu, J. Lu and B. Huang, Electronic and magnetic properties of perfect, vacancy-doped, and nonmetal adsorbed MoSe$_2$, MoTe$_2$ and WS$_2$ monolayers, *Phys. Chem. Chem. Phys.*, 2011, **13**(34), 15546.

46 Y. Li, X. Zhang, D. Chen, S. Xiao and J. Tang, Adsorption behavior of COF$_2$ and CF$_4$ gas on the MoS$_2$ monolayer doped with Ni: a first-principles study, *Appl. Surf. Sci.*, 2018, 443.

47 X. Zhang, H. Cui, D. Chen, X. Dong and J. Tang, Electronic structure and H$_2$S adsorption property of Pt$_3$ cluster decorated (8, 0) SWCNT, *Appl. Surf. Sci.*, 2018, 428.

48 M. D. Ganji, N. Sharifi, M. Ardjmand and G. A. Morteza, Pt-decorated graphene as superior media for H$_2$S adsorption: a first-principles study, *Appl. Surf. Sci.*, 2012, **261**(3), 697–704.

49 P. Pyykkö and M. Atsumi, Molecular single-bond covalent radii for elements 1-118, *Chemistry*, 2009, **15**(1), 186–197.

50 A. J. Yang, D. W. Wang, H. W. Xiao, J. F. Chu, P. L. Lv, Y. Liu and Z. R. Ming, Phosphorene: A Promising Candidate for Highly Sensitive and Selective SF$_6$ Decomposition Gas Sensors, *IEEE Electron Device Lett.*, 2017, **38**(7), 963–966.

51 S. W. Han, G. B. Cha, Y. Park and S. C. Hong, Hydrogen physisorption based on the dissociative hydrogen chemisorption at the sulphur vacancy of MoS$_2$ surface, *Sci. Rep.*, 2017, **7**(1), 7152–7158.

52 W. Wei, Y. Dai and B. Huang, In-plane interfacing effects of two-dimensional transition-metal dichalcogenide heterostructures, *Phys. Chem. Chem. Phys.*, 2016, **18**(23), 15632–15638.

53 H. Cui, Q. Li, G. Qiu and J. Wang, Carbon-chain inserting effect on electronic behavior of single-walled carbon nanotubes: a density functional theory study, *MRS Commun.*, 2018, **8**(1), 189–193.

54 F. Schedin, A. K. Geim, S. V. Morozov, E. W. Hill, P. Blake, M. I. Katnelson and K. S. Novoselov, Detection of individual gas molecules adsorbed on graphene, *Nat. Mater.*, 2007, **6**(9), 652–655.

55 Y. H. Zhang, Y. B. Chen, K. G. Zhou, C. H. Liu, J. Zeng, H. L. Zhang and Y. Peng, Improving gas sensing properties of graphene by introducing dopants and defects: a first-principles study, *Nanotechnology*, 2009, **20**(18), 185504.

56 S. Peng, K. Cho, P. Qi and H. Dai, *Ab initio* study of CNT NO$_2$ gas sensor, *Chem. Phys. Lett.*, 2004, **387**(4), 271–276.

57 H. Cui, K. Zheng, Y. Zhang, H. Ye and X. Chen, Superior Selectivity and Sensitivity of C$_3$N Sensor in Probing Toxic Gases NO$_2$ and SO$_2$, *IEEE Electron Device Lett.*, 2018, **39**(2), 284–287.

58 M. Sharma, P. Jamdagni, A. Kumar and P. K. Ahluwalia, Interactions of gas molecules with monolayer MoSe$_2$: a first principle study, *AIP Conf. Proc.*, 2016, 52903.

59 H. Qin, F. Chuang, X. Luan and D. Yang, First-principles investigation of adsorption behaviors of small molecules on penta-graphene, *Nanoscale Res. Lett.*, 2018, **13**(1), 264.

60 H. Wei, Y. Gui, J. Kang, W. Wang and C. Tang, A DFT Study on the Adsorption of H$_2$S and SO$_2$ on Ni Doped MoS$_2$ Monolayer, *Nanomaterials*, 2018, 646–657.

61 B. Zhao, C. Y. Li, L. L. Liu, B. Zhou, Q. K. Zhang, Z. Q. Chen and Z. Tang, Adsorption of gas molecules on Cu impurities embedded monolayer MoS$_2$: a first-principles study, *Appl. Surf. Sci.*, 2016, **382**, 280–287.

62 H. Cui, X. Zhang and D. Chen, Borophene: a promising adsorbent material with strong ability and capacity for SO$_2$ adsorption, *Appl. Phys. A: Mater. Sci. Process.*, 2018, **124**(9), 636.